RESEARCH ARTICLE | SEPTEMBER 26 2023

Ultrathin superconducting TaC_xN_{1-x} films prepared by plasma-enhanced atomic layer deposition with ion-energy control

Silke A. Peeters ; Ciaran T. Lennon ; Marc J. M. Merkx ; Robert H. Hadfield ; W. M. M. (Erwin) Kessels ; Marcel A. Verheijen ; Harm C. M. Knoops

Appl. Phys. Lett. 123, 132603 (2023)
https://doi.org/10.1063/5.0169339

Applied Physics Letters ARTICLE pubs.aip.org/aip/apl

Ultrathin superconducting TaC_xN_{1-x} films prepared by plasma-enhanced atomic layer deposition with ion-energy control

Cite as: Appl. Phys. Lett. **123**, 132603 (2023); doi: 10.1063/5.0169339
Submitted: 25 July 2023 · Accepted: 12 September 2023 ·
Published Online: 26 September 2023

Silke A. Peeters,[1,a)] Ciaran T. Lennon,[2] Marc J. M. Merkx,[1] Robert H. Hadfield,[2] W. M. M. (Erwin) Kessels,[1] Marcel A. Verheijen,[1,3] and Harm C. M. Knoops[1,4,a)]

AFFILIATIONS

[1]Eindhoven University of Technology, P.O. Box 513, 5600 MB Eindhoven, The Netherlands
[2]James Watt School of Engineering, University of Glasgow, Glasgow G12 8QQ, United Kingdom
[3]Eurofins Materials Science, High Tech Campus 11, 5656 AE Eindhoven, The Netherlands
[4]Oxford Instruments Plasma Technology, North End, Bristol, BS49 4AP, United Kingdom

[a)]**Authors to whom correspondence should be addressed:** s.a.peeters@tue.nl and h.c.m.knoops@tue.nl

ABSTRACT

This work demonstrates that plasma-enhanced atomic layer deposition (PEALD) with substrate biasing enables the preparation of ultrathin superconducting TaC_xN_{1-x} films. By comparing with films grown without substrate biasing, the enhanced ion energies yield a hundredfold reduction in room-temperature resistivity: a comparably low value of 217 $\mu\Omega$ cm is obtained for a 40 nm film. The ion-energy control enables tuning of the composition, counteracts oxygen impurity incorporation, and promotes a larger grain size. Correspondingly, the critical temperature of superconductivity (T_c) displays clear ion-energy dependence. With optimized ion energies, a consistently high T_c around 7 K is measured down to 11 nm film thickness. These results demonstrate the high ultrathin-film quality achievable through PEALD combined with substrate biasing. This process is particularly promising for the fabrication of low-loss superconducting quantum devices.

Superconducting quantum circuits are among the leading architectures implemented in the current noisy, intermediate-scale quantum technology.[1,2] At the same time, it is recognized that the transition to large-scale, fault-tolerant systems can only be realized through major material advances and the development of scalable fabrication methods.[1,2] Miniaturization and dense integration of circuit features, which itself is limited by material defects, is also key for the performance and scalability of these systems.[3,4]

Atomic layer deposition (ALD) is very promising in this context for its true atomic-scale control and compatibility with large-scale fabrication.[5] ALD has become a well-established thin-film deposition technique nowadays widely applied in the semiconductor industry. Motivated by the challenges in the preparation of quantum devices, ALD of superconducting materials has been explored in recent years, albeit to a limited extent.[6–8] The studies generally focus on refractory metal-nitrides, mostly NbN, which are of particular interest due to their typically higher oxidation resistance[9,10] and critical temperatures[11–13] compared to their pure-metal counterparts. However, obtaining highly conductive metal-nitrides through ALD remains challenging.[14,15]

Using a plasma in the ALD process is often shown to allow for the growth of conductive films.[14,15] As previously demonstrated by our research, plasma-enhanced ALD (PEALD) with radio frequency (RF) substrate biasing can significantly improve film quality by providing ion-energy control that enables the tuning of material properties.[14,16,17] Examples of beneficial effects of enhanced ion energies are film densification, increased electrical conductivity, and reduced impurity contents. Similar benefits of energetic ions have been observed in physical vapor deposition techniques[18] commonly used to prepare superconducting films.[19–21] Combined with the unique merits of PEALD, energetic ions could be key enablers of low-loss quantum circuits with ultrathin superconducting components.

In this Letter, we demonstrate that enhanced ion energies are essential for the preparation of high-quality, ultrathin superconducting TaC_xN_{1-x} films by PEALD. The choice for TaC_xN_{1-x} is inspired by the record coherence times achieved with Ta superconducting

transmon qubits.[20,21] We assess the TaC_xN_{1-x} film quality through investigations of the room-temperature conductivity, atomic composition, and microstructure of the films and show that ion-energy control is key in tailoring these properties. We demonstrate superconductivity in 7–40 nm thick TaC_xN_{1-x} with high critical temperatures sustained down to 11 nm film thickness.

Thin TaC_xN_{1-x} films were prepared on Si(100) substrates at a substrate table temperature of 250 °C by PEALD on an Oxford Instruments FlexAL system. All depositions included both 10–20 Ωcm n-type Si(100) with 1–2 nm native oxide and with 450 nm thermal oxide. Some deposition runs included also high-resistivity (>10 kΩcm) Si(100) substrates with 1–2 nm native oxide. Together with sapphire, high-resistivity Si is the conventionally used substrate for superconducting quantum devices.[22] The used precursor was $Ta[N(CH_3)_2]_3[NC(CH_3)_3]$ [(tert-butylimino)tris(dimethylamino)tantalum, or TBTDMT] and the gas flow through the plasma source consisted of 10/40 sccm Ar/H_2 resulting in a 6 mTorr pressure during the plasma half-cycle. The remote plasma was generated by an inductively coupled plasma (ICP) source operated at a power of 100 W at radio frequency (13.56 MHz). The ion energy was controlled via substrate biasing: a second radio frequency (13.56 MHz) power supply was connected to the substrate table. By varying the biasing power, the voltage over the plasma sheath could be controlled and the energy of the ions impacting the film could be enhanced. Bias powers between 0 W (grounded table) and 35 W were used, leading to average ion energies in the range of 20–250 eV.[16] Further details on the PEALD process, including ion flux-energy distribution functions and saturation curves, can be found in Sec. S1 of the supplementary material.

To assess the suitability of the prepared films for superconducting quantum circuits, the film properties are studied as a function of film thickness (Figs. 1 and 3) and applied RF bias power (Figs. 2 and 3, and Table I). Film thicknesses are determined by *ex situ* spectroscopic ellipsometry (SE), which is combined with four-point probe (FPP) measurements on Si(100) substrates with thermal oxide to obtain the resistivity. X-ray reflectivity (XRR) is used to confirm the thicknesses obtained through SE and to determine the mass density. The film composition is investigated by x-ray photoelectron spectroscopy (XPS) and elastic (non-Rutherford) backscattering spectrometry (EBS). The crystal structure is studied through scanning transmission electron microscopy (STEM) imaging, top-view electron diffraction, and x-ray diffraction (XRD). The surface roughness is extracted from atomic force microscopy (AFM) measurements. The methods are further elaborated on in Sec. S2 of the supplementary material.

For the preparation of TaC_xN_{1-x} films of varying thickness between 7 and 40 nm, a 20 W RF bias power is applied to the substrate. FPP measurements reveal a persistently low lateral room-temperature resistivity, which decreases with increasing film thickness [Fig. 1(a)]. For 40 nm films, a 217 ± 7 μΩ cm resistivity is measured, which is relatively low for tantalum (carbo)nitride films with thickness below 1 μm.[25–28] Due to the low bulk resistivities of both TaC (22 μΩ cm[29]) and TaN (180 μΩ cm[29]), excellent conductivity can be achieved for the TaC_xN_{1-x} films. The low resistivity of the films can be understood from their stoichiometric TaC_xN_{1-x} composition with $x = 0.42 \pm 0.04$, negligible oxygen impurity content, and high mass density of 13.4 ± 0.2 g cm^{-3} (Table I). In addition, as seen from the cross-sectional BF-STEM inset image in Fig. 1(a), a smooth, closed film is obtained. The grains appear to extend across the film, up from

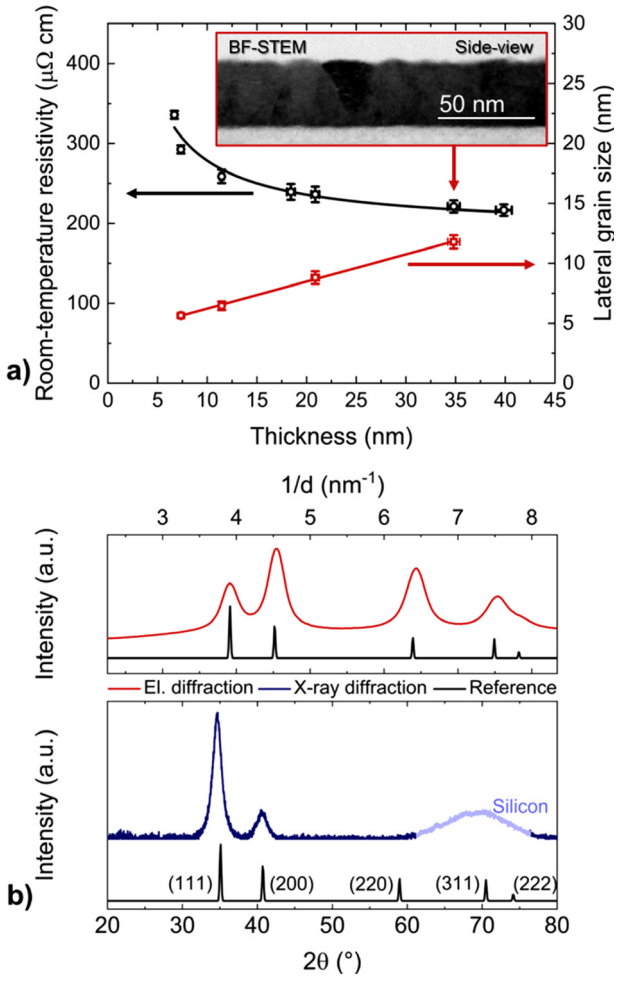

FIG. 1. (a) Lateral room-temperature resistivity and grain size for a range of film thicknesses of TaC_xN_{1-x} prepared with 20 W RF bias power. The resistivity data are fitted with a grain boundary scattering model[23] (supplementary material S2.2), and the lateral grain size is fitted with a linear relation. A BF-STEM image of a cross section of a 35 nm film is shown in the inset. (b) Radially averaged intensity curve extracted from the electron diffraction pattern in supplementary material S2.6 and gonio-mode x-ray diffractogram (with 3° axis offset) of a 35 nm film. The peaks are identified by the TaC_xN_{1-x} fcc orientations, referenced to powder diffractograms [ICSD ID 108168 (Ref. 24), black peaks], with an additional peak due to the Si (100) substrate in the x-ray diffractogram.

the thin (∼1 to 2 nm) amorphous native oxide layer at the substrate interface. From the sloping grain boundaries, it is observed that the lateral grain size increases linearly as a function of film thickness. This is confirmed by determination of the average lateral grain size from top-view STEM images (supplementary material S2.6) of films of various thicknesses [red curve in Fig. 1(a)]. This yields an average 11.8 ± 0.6 nm grain size for 35 nm film thickness.

The crystal structure is studied by XRD and top-view electron diffraction. The x-ray diffractogram and radially averaged electron diffraction intensity curve of Fig. 1(b) correspond to a face-centered cubic (fcc) polycrystalline structure, confirming the growth of single-phase TaC_xN_{1-x}. Though fcc TaN is metastable, this phase can be formed

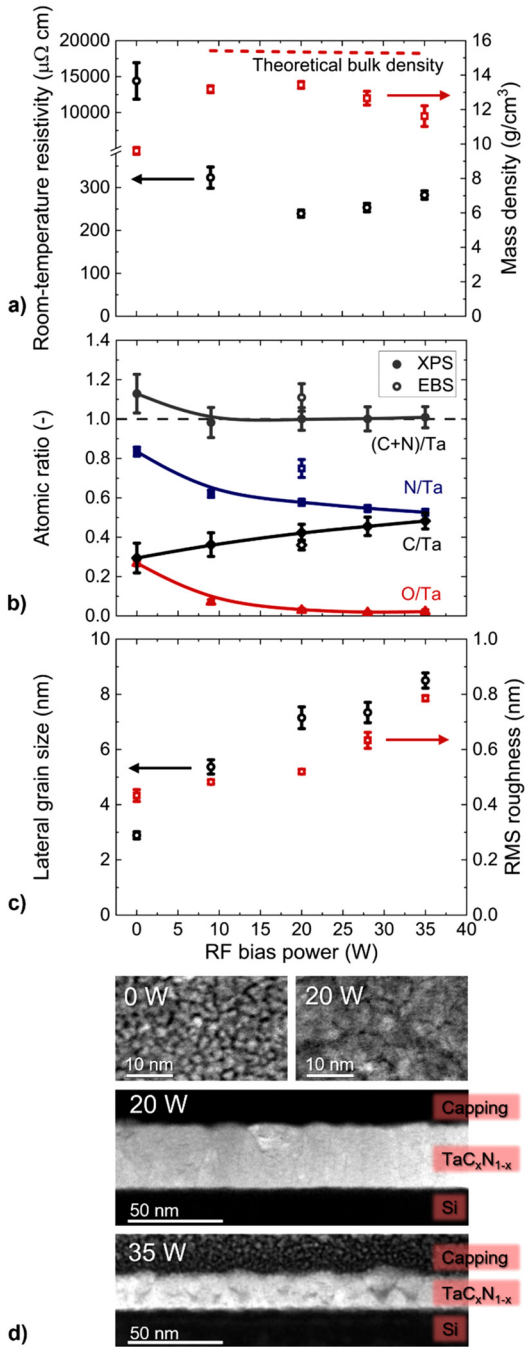

FIG. 2. (a) Room-temperature resistivity (black) and mass density (red) of TaC_xN_{1-x} films of ~19 nm thickness for various applied RF bias powers. The theoretical bulk density is indicated for the stoichiometric films by the red dashed line (calculated from ICSD 159875 and 76456). (b) Atomic ratios measured by XPS (closed symbols), with guides to the eye, and EBS (open symbols). (c) Lateral grain size (black) and RMS surface roughness (red). (d) Top-view HAADF-STEM images for films prepared with 0 and 20 W RF bias power and cross-sectional HAADF-STEM images for films prepared with 20 and 35 W RF bias power, where the capping layer is prepared by electron beam-induced deposition. The values of film thicknesses, varying between 11 and 35 nm, are listed in supplementary material S2.1.

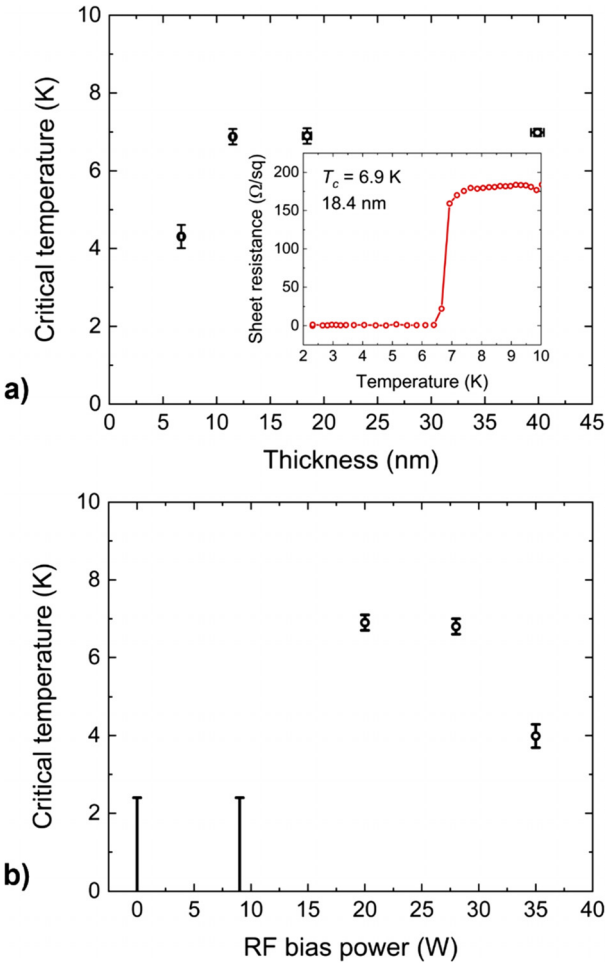

FIG. 3. (a) Critical temperature for TaC_xN_{1-x} films prepared with 20 W RF bias power for a range of film thicknesses. The inset shows the superconducting transition recorded for the 18 nm TaC_xN_{1-x} film. (b) Dependence of the critical temperature of TaC_xN_{1-x} films of ~19 nm thickness on the RF bias power. At low bias powers, the error bars indicate that no superconducting transition was measured above a temperature of 2.4 K.

through the energy supplied by the energetic ions during film growth,[30,31] enabling the growth of a cubic solid–solid solution of fcc TaC and TaN.[10,26,32] The continuous fcc TaC_xN_{1-x} crystal structure is desirable not only due to its large range of possible compositions,[10,33] but also because it is the only TaC_xN_{1-x} crystal structure reported to superconduct above 1.5 K.[33,34]

The effect of energetic ions on the conductivity, composition, and microstructure is reported in Fig. 2 and Table I. Varying the RF bias power applied to the substrate between 0 and 35 W reveals a hundredfold reduction in room-temperature resistivity through substrate biasing [Fig. 2(a)]. The large drop in resistivity can be related to both changes in film microstructure and composition. Though all films grown in this work are of the fcc structure (as shown in the supplementary material S2.7), the microstructure is greatly affected by the high-energy ions. The impact of energetic ions during film growth results in an enhanced mass-density [Fig. 2(a)] and promotes grain

TABLE I. Summary of growth per cycle (GPC) values and material properties for TaC_xN_{1-x} films prepared with a 0 and 20 W RF bias power. The film thicknesses are 18.8 and 20.9 nm, respectively.

	0 W RF bias power	20 W RF bias power
GPC (thickness)	0.55 ± 0.03 Å	0.35 ± 0.03 Å
GPC (Ta areal density)[a]	1.36 ± 0.04 at. nm^{-2}	1.23 ± 0.03 at. nm^{-2}
Resistivity	$(1.4 \pm 0.1) \times 10^4$ μΩ cm	236 ± 10 μΩ cm
Mass density	10.2 ± 0.3 g cm^{-3}	13.4 ± 0.2 g cm^{-3}
Lateral grain size	2.9 ± 0.1 nm	7.2 ± 0.4 nm
RMS roughness	0.43 ± 0.02 nm	0.520 ± 0.007 nm
N/Ta[b]	0.83 ± 0.02	0.58 ± 0.02
C/Ta[b]	0.29 ± 0.08	0.42 ± 0.04
O[b]	10 ± 2 at.%	≤ 2 at.%
Ar[a]	< 0.1 at.%	0.7 ± 0.3 at.%

[a]Derived from EBS measurements.
[b]Derived from XPS measurements, top and substrate interface regions excluded.

growth [Fig. 2(c)] as determined from XRR measurements and top-view STEM images (supplementary material S2.6), respectively. This is also seen in the top-view HAADF-STEM images of Fig. 2(d), where a less dense layer is grown without substrate biasing (0 W), while more energetic ions (20 W) yield larger grain sizes. It is likely that energetic ions promote grain coalescence during film growth, as has often been attributed to increased mobility of surface species.[17,18] XPS measurements [Fig. 2(b)] indicate films grown without substrate biasing contain notable oxygen impurities (10 at. % in Table I), whereas oxygen contents are negligible for enhanced ion energies. As a consequence, energetic ions enable the growth of stoichiometric TaC_xN_{1-x} films. Furthermore, substrate biasing provides some tunability of the TaC_xN_{1-x} composition; x increases from 0.36 for 9 W RF bias power to 0.48 for 35 W RF bias power. The improved conductivity, microstructure, and composition confirm film-quality enhancement through energetic ions. Similar beneficial effects of energetic ions in PEALD have been observed for other conductive metal-nitrides (HfN_x[14,17] and TiN_x[17]) in our previous studies. Though we do not observe a beneficial effect of energetic ions on the root mean square (RMS) surface roughness [Fig. 2(c)] as determined by AFM, it remains below 1 nm, confirming the growth of smooth films. In addition to the beneficial effect of energetic ions, Fig. 2 demonstrates the importance of ion-energy control. For excessive ion-energy enhancement, we observe an onset of material degradation, specifically in resistivity and mass density. The theoretical bulk density, which was calculated assuming a linear relation between the C/N ratio and density that has been reported for the fcc TaC_xN_{1-x} system,[26] is indicated by the red dashed line in Fig. 2(a). Comparing the theoretical and measured mass density we observe that the measured mass density decreases more strongly than expected from this linear relation, indicating material degradation beyond ∼20 W RF bias power. This is confirmed by the cross-sectional HAADF-STEM images of Fig. 2(d), which reveal voids in the film prepared with 35 W RF bias power. A similar trend of ion-induced damage was also observed in our earlier work on PEALD with substrate biasing.[17] When their energy is too high, the ions can lead to significant void incorporation, implantation, which occurs to a small extent by Ar in the studied films, see Table I, and creation of a large number of vacancies, interstitials, and dislocations by atomic displacements during film growth.[17,35]

Finally, we confirm superconductivity of the films through FPP measurements on high-resistivity Si(100) substrates at sample temperatures between 2.4 and 300 K. We measure a consistently high critical temperature (T_c) of 7 K for the 11–40 nm films prepared with 20 W bias power [Fig. 3(a)]. A relatively high T_c for such thin films is a rarity, and has only been achieved for TaN grown by high-temperature sputtering on sapphire substrates.[36,37] For the 6.7 nm film in Fig. 3(a), the T_c decreases to 4.3 K, as expected from the increase in room-temperature resistivity observed in Fig. 1(a). Moreover, the 6.7 nm film thickness is likely slightly below the coherence length of the material.[38] The confirmed superconducting transition for such a thin film and the high T_c sustained down to 11 nm point to the high quality achievable for ultrathin films through PEALD.

The effect of energetic ions on the T_c is depicted in Fig. 3(b), which indicates an optimum ion energy. For films prepared with 0 and 9 W bias powers, no superconducting transition is recorded. High T_c values around 7 K are observed for 20 and 28 W bias powers, after which the T_c degrades to 4 K for 35 W bias power. These results are in agreement with the ion-energy-dependence of the properties in Fig. 2, underlining the importance of achieving low impurity levels, small grain boundary area, and minor microstructural damage. It follows that ion-energy control is critical for the preparation of ultrathin films with high T_c by PEALD.

In conclusion, we have assessed the suitability of the prepared films for superconducting quantum circuits through investigation of their electrical conductivity, composition, and microstructure. Energetic ions enhance conductivity, purity, density, and T_c in TaC_xN_{1-x} films prepared by PEALD and in this way enable the growth of superconducting TaC_xN_{1-x} films down to 7 nm film thickness. In addition, a high smoothness of PEALD films is demonstrated. These material properties are promising for integration of the films in superconducting quantum circuits, where high-quality material and interfaces are key. Also taking into account scalability and reproducibility, PEALD with substrate biasing could become an enabling technique for low-loss quantum circuits with ultrathin superconducting

components. For thin-film applications where some film disorder is desired, such as superconducting nanowire single photon detectors (SNSPDs),[39,40] the high-energy regime of PEALD with substrate biasing holds much promise as well.

See the supplementary material for the PEALD process details, elaboration on characterization techniques, film thicknesses, fit of the thickness-dependence of the room-temperature resistivity, additional XPS data, HAADF-STEM images, and electron diffraction and x-ray diffraction measurements.

This work has been carried out within the Open Technology Program with Project No. 19438, which is financed by the Netherlands Organization for Scientific Research (NWO). The authors gratefully acknowledge Rik Lengers (TU/e), Rik Heinemans (TU/e), and Dr. Yi Shu (OIPT) for their work on developing the PEALD process; Dr. Wim Arnold Bik (Detect99) for performing the EBS measurements; Caspar van Bommel, Janneke Zeebregts, Barathi Krishnamoorthy for technical support at TU/e; and Cristian van Helvoirt and Dr. Beatriz Barcones (TU/e) for FIB preparation of TEM samples. Solliance and the Dutch province of Noord-Brabant are acknowledged for funding the TEM facility. We are thankful to Arthur de Jong (TU/e) for XPS uncertainty analysis and Dr. Miika Mattinen (TU/e) for insightful discussion.

Robert Hadfield acknowledges support from the UK Engineering & Physical Sciences Research Council (EPSRC - Project Nos. EP/W032627/1, EP/S026428/1, and EP/T00097X/1) and the UK Science and Technologies Facilities Council (STFC - Project No. ST/T005920/1). Ciaran Lennon acknowledges support from the EPSRC Center for Doctoral Training in Intelligent Sensing and Measurement (CDT-ISM) (Grant No. EP/L016753/1) and industrial sponsorship from Oxford Instruments Plasma Technology (OIPT).

AUTHOR DECLARATIONS

Conflict of Interest

The authors have no conflicts to disclose.

Author Contributions

Silke A. Peeters: Conceptualization (supporting); Formal analysis (lead); Methodology (equal); Visualization (lead); Writing – original draft (lead); Writing – review & editing (lead). **Ciaran T. Lennon:** Formal analysis (supporting); Methodology (equal); Writing – review & editing (supporting). **M. J. M. Merkx:** Formal analysis (supporting); Methodology (equal); Writing – review & editing (supporting). **Robert H. Hadfield:** Supervision (equal); Writing – review & editing (supporting). **W. M. M. Kessels:** Conceptualization (equal); Funding acquisition (equal); Supervision (equal); Writing – review & editing (equal). **M. A. Verheijen:** Formal analysis (supporting); Methodology (equal); Writing – review & editing (supporting). **H. C. M. Knoops:** Conceptualization (equal); Funding acquisition (equal); Supervision (equal); Writing – review & editing (equal).

DATA AVAILABILITY

The data that support the findings of this study are available within the article and its supplementary material.

REFERENCES

[1]N. P. de Leon, K. M. Itoh, D. Kim, K. K. Mehta, T. E. Northup, H. Paik, B. S. Palmer, N. Samarth, S. Sangtawesin, and D. W. Steuerman, "Materials challenges and opportunities for quantum computing hardware," Science **372**, eabb2823 (2021).
[2]W. D. Oliver and P. B. Welander, "Materials in superconducting quantum bits," MRS Bull. **38**, 816–825 (2013).
[3]J. I. Wang, M. A. Yamoah, Q. Li, A. H. Karamlou, T. Dinh, B. Kannan, J. Braumüller, D. Kim, A. J. Melville, S. E. Muschinske *et al.*, "Hexagonal boron nitride as a low-loss dielectric for superconducting quantum circuits and qubits," Nat. Mater. **21**, 398–403 (2022).
[4]C. R. H. McRae, H. Wang, J. Gao, M. R. Vissers, T. Brecht, A. Dunsworth, D. P. Pappas, and J. Mutus, "Materials loss measurements using superconducting microwave resonators," Rev. Sci. Instrum. **91**, 091101 (2020).
[5]R. W. Johnson, A. Hultqvist, and S. F. Bent, "A brief review of atomic layer deposition: From fundamentals to applications," Mater. Today **17**, 236–246 (2014).
[6]C. Sheagren, P. Barry, E. Shirokoff, and Q. Y. Tang, "Atomic layer deposition niobium nitride films for high-Q resonators," J. Low Temp. Phys. **199**, 875–882 (2020).
[7]A. Shearrow, G. Koolstra, S. J. Whiteley, N. Earnest, P. S. Barry, F. J. Heremans, D. D. Awschalom, E. Shirokoff, and D. I. Schuster, "Atomic layer deposition of titanium nitride for quantum circuits," Appl. Phys. Lett. **113**, 212601 (2018).
[8]G. G. Taylor, D. V. Morozov, C. T. Lennon, P. S. Barry, C. Sheagren, and R. H. Hadfield, "Infrared single-photon sensitivity in atomic layer deposited superconducting nanowires," Appl. Phys. Lett. **118**, 191106 (2021).
[9]C. Müller, J. H. Cole, and J. Lisenfeld, "Towards understanding two-level-systems in amorphous solids: Insights from quantum circuits," Rep. Prog. Phys. **82**, 124501 (2019).
[10]J. K. Schaeffer, C. Capasso, R. Gregory, D. Gilmer, L. R. C. Fonseca, M. Raymond, C. Happ, M. Kottke, S. B. Samavedam, P. J. Tobin *et al.*, "Tantalum carbonitride electrodes and the impact of interface chemistry on device characteristics," J. Appl. Phys. **101**, 014503 (2007).
[11]F. M. Kilbane and P. S. Habig, "Superconducting transition temperatures of reactively sputtered films of tantalum nitride and tungsten nitride," J. Vac. Sci. Technol. **12**, 107–109 (1975).
[12]B. T. Matthias, T. H. Geballe, and V. B. Compton, "Superconductivity," Rev. Mod. Phys. **35**, 1–22 (1963).
[13]D. R. Slocombe, V. L. Kuznetsov, W. Grochala, R. J. P. Williams, and P. P. Edwards, "Superconductivity in transition metals," Philos. Trans. R. Soc., A **373**, 20140476 (2015).
[14]S. Karwal, B. Karasulu, H. C. M. Knoops, V. Vandalon, W, M. M. Kessels, and M. Creatore, "Atomic insights into the oxygen incorporation in atomic layer deposited conductive nitrides and its mitigation by energetic ions," Nanoscale **13**, 10092–10099 (2021).
[15]H. C. M. Knoops, T. Faraz, K. Arts, and W. M. M. Kessels, "Status and prospects of plasma-assisted atomic layer deposition," J. Vac. Sci. Technol., A **37**, 030902 (2019).
[16]S. Karwal, M. A. Verheijen, K. Arts, T. Faraz, W. M. M. Kessels, and M. Creatore, "Plasma-assisted ALD of highly conductive HfN_x: On the effect of energetic ions on film microstructure," Plasma Chem. Plasma Process. **40**, 697–712 (2020).
[17]T. Faraz, H. C. M. Knoops, M. A. Verheijen, C. A. A. Van Helvoirt, S. Karwal, A. Sharma, V. Beladiya, A. Szeghalmi, D. M. Hausmann, J. Henri *et al.*, "Tuning material properties of oxides and nitrides by substrate biasing during plasma-enhanced atomic layer deposition on planar and 3D substrate topographies," ACS Appl. Mater. Interfaces **10**, 13158–13180 (2018).
[18]I. Petrov, P. B. Barna, L. Hultman, and J. E. Greene, "Microstructural evolution during film growth," J. Vac. Sci. Technol., A **21**, S117–S128 (2003).
[19]C.-B. Eom and J. M. Murduck, "Synthesis and characterization of superconducting thin films," Thin Films **28**, 227–270 (2001).
[20]A. P. M. Place, L. V. H, Rodgers, P. Mundada, B. M. Smitham, M. Fitzpatrick, Z. Leng, A. Premkumar, J. Bryon, A. Vrajitoarea, S. Sussman *et al.*, "New material platform for superconducting transmon qubits with coherence times exceeding 0.3 milliseconds," Nat. Commun. **12**, 1779 (2021).

[21]C. Wang, X. Li, H. Xu, Z. Li, J. Wang, Z. Yang, Z. Mi, X. Liang, T. Su, C. Yang *et al.*, "Towards practical quantum computers: Transmon qubit with a lifetime approaching 0.5 milliseconds," npj Quantum Inf. **8**, 3 (2022).
[22]C. E. Murray, "Material matters in superconducting qubits," Mater. Sci. Eng., R **146**, 100646 (2021).
[23]A. F. Mayadas and M. Shatzkes, "Electrical-resistivity model for polycrystalline films: The case of arbitrary reflection at external surfaces," Phys. Rev. B **1**, 1382 (1970).
[24]J. Gatterer, G. Dufek, P. Ettmayer, and R. Kieffer, "Das kubische Tantalmononitrid (B 1-Typ) und seine Mischbarkeit mit den isotypen Übergangsmetallnitriden und-carbiden," Monatsh. Chem. **106**, 1137–1147 (1975).
[25]E. Langereis, H. C. M. Knoops, A. J. M. Mackus, F. Roozeboom, M. C. M. Van de Sanden, and W. M. M. Kessels, "Synthesis and in situ characterization of low-resistivity TaN_x films by remote plasma atomic layer deposition," J. Appl. Phys. **102**, 083517 (2007).
[26]C. Hossbach, S. Teichert, J. Thomas, L. Wilde, H. Wojcik, D. Schmidt, B. Adolphi, M. Bertram, U. Mühle, M. Albert *et al.*, "Properties of plasma-enhanced atomic layer deposition-grown tantalum carbonitride thin films," J. Electrochem. Soc. **156**, H852 (2009).
[27]N. D. Cuong, D.-J. Kim, B.-D. Kang, C. S. Kim, K.-M. Yu, and S.-G. Yoon, "Characterization of tantalum nitride thin films deposited on SiO_2/Si substrates using dc magnetron sputtering for thin film resistors," J. Electrochem. Soc. **153**, G164 (2006).
[28]C.-C. Chang, J. S. Jeng, and J.-S. Chen, "Microstructural and electrical characteristics of reactively sputtered Ta-N thin films," Thin Solid Films **413**, 46–51 (2002).
[29]E. R. Engbrecht, Y.-M. Sun, S. Smith, K. Pfiefer, J. Bennett, J. M. White, and J. G. Ekerdt, "Chemical vapor deposition growth and properties of Tac_xN_y," Thin Solid Films **418**, 145–150 (2002).
[30]S. Chaudhuri, I. J. Maasilta, L. Chandernagor, M. Ging, and M. Lahtinen, "Fabrication of superconducting tantalum nitride thin films using infrared pulsed laser deposition," J. Vac. Sci. Technol., A **31**, 061502 (2013).
[31]W. Ensinger, M. Kiuchi, and M. Satou, "Low-temperature formation of metastable cubic tantalum nitride by metal condensation under ion irradiation," J. Appl. Phys. **77**, 6630–6635 (1995).
[32]A. A. Lavrentyev, B. V. Gabrelian, V. B. Vorzhev, I. Y. Nikiforov, and O. Y. Khyzhun, "Electronic properties of cubic TaC_xN_{1-x}: A comparative study using self-consistent cluster and ab initio band-structure calculations and x-ray spectroscopy," J. Alloys Compd. **472**, 104–111 (2009).
[33]E. Thorwarth, M. Dietrich, and C. Politis, "Superconducting and normal state properties of tantalumcarbonitrides under hydrostatic pressure," Solid State Commun. **20**, 869–872 (1976).
[34]D. Gerstenberg and P. M. Hall, "Superconducting thin films of niobium, tantalum, tantalum nitride, tantalum carbide, and niobium nitride," J. Electrochem. Soc. **111**, 936 (1964).
[35]R. Gago, I. Jiménez, and J. M. Albella, *Thin Film Growth by Ion-Beam-Assisted Deposition Techniques* (Elsevier Amsterdam, The Netherlands, 2006), Vol. 63.
[36]A. Engel, A. Aeschbacher, K. Inderbitzin, A. Schilling, K. Il'in, M. Hofherr, M. Siegel, A. Semenov, and H.-W. Hübers, "Tantalum nitride superconducting single-photon detectors with low cut-off energy," Appl. Phys. Lett. **100**, 062601 (2012).
[37]R. Lusche, A. Semenov, K. Ilin, M. Siegel, Y. Korneeva, A. Trifonov, A. Korneev, G. Goltsman, D. Vodolazov, and H.-W. Hübers, "Effect of the wire width on the intrinsic detection efficiency of superconducting-nanowire single-photon detectors," J. Appl. Phys. **116**, 043906 (2014).
[38]N. P. Breznay, K. Michaeli, K. S. Tikhonov, A. M. Finkel'Stein, M. Tendulkar, and A. Kapitulnik, "Hall conductivity dominated by fluctuations near the superconducting transition in disordered thin films," Phys. Rev. B **86**, 014514 (2012).
[39]I. Holzman and Y. Ivry, "Superconducting nanowires for single-photon detection: Progress, challenges, and opportunities," Adv. Quantum Technol. **2**, 1800058 (2019).
[40]D. V. Morozov, A. Casaburi, and R. H. Hadfield, "Superconducting photon detectors," Contemp. Phys. **62**, 69–91 (2021).